Squeezing and quantum approximate optimization

Gopal Chandra Santra [1,2,*] Fred Jendrzejewski [1,3] Philipp Hauke [2,4] and Daniel J. Egger [5]

[1]*Kirchhoff-Institut für Physik, Universität Heidelberg, Im Neuenheimer Feld 227, 69120 Heidelberg, Germany*
[2]*Pitaevskii BEC Center and Department of Physics, University of Trento, Via Sommarive 14, I-38123 Trento, Italy*
[3]*Alqor UG (haftungsbeschränkt), Marquardstrasse 46, 60489 Frankfurt am Main, Germany*
[4]*INFN-TIFPA, Trento Institute for Fundamental Physics and Applications, Via Sommarive 14, I-38123 Trento, Italy*
[5]*IBM Quantum, IBM Research Europe - Zurich, Säumerstrasse 4, CH-8803 Rüschlikon, Switzerland*

Variational quantum algorithms offer fascinating prospects for the solution of combinatorial optimization problems using digital quantum computers. However, the achievable performance in such algorithms and the role of quantum correlations therein remain unclear. Here, we shed light on this open issue by establishing a tight connection to the seemingly unrelated field of quantum metrology: Metrological applications employ quantum states of spin ensembles with a reduced variance to achieve an increased sensitivity, and we cast the generation of such squeezed states in the form of finding optimal solutions to a combinatorial MaxCut problem with an increased precision. By solving this optimization problem with a quantum approximate optimization algorithm (QAOA), we show numerically as well as on an IBM Quantum chip how highly squeezed states are generated in a systematic procedure that can be adapted to a wide variety of quantum machines. Moreover, squeezing tailored for the QAOA of the MaxCut permits us to propose a figure of merit for future hardware benchmarks. Exploiting the connection, we show how the performance can be improved by warm-starting the optimization algorithm with the squeezed state.

I. INTRODUCTION

The quantum approximate optimization algorithm (QAOA) [1] is a promising approach for solving combinatorial optimization problems using digital quantum computers [2,3]. In this framework, combinatorial problems such as the MaxCut and MAX-SAT are mapped to the task of finding the ground state of an Ising Hamiltonian [4–6]. QAOA uses constructive interference to find solution states [7], and it has better performance than finite-time adiabatic evolution [8]. However, it remains an outstanding challenge to characterize the role of quantum effects such as entanglement in QAOA.

Here, we show how concepts from quantum metrology shed light onto the influence of squeezing and entanglement in the performance of QAOA. Illustratively, the connection is established through the insight that (a) the aim of QAOA is to obtain the ground state as precisely as possible, while (b) quantum metrology leverages entanglement between particles to generate states that permit precision beyond the capacities of any comparable classical sensor [9–11]. For example, squeezed states can increase sensitivity for detecting phases [12], magnetic fields [13], and gravitational waves [14]. The most sensitive states for phase estimation are Dicke states [10,15], where all qubits are equally entangled. We substantiate this connection through numerically exact calculations and data gathered on IBM Quantum hardware with up to eight qubits. Our analysis shows how the search for an optimal solution to the MaxCut problem on a complete graph through QAOA generates Dicke states, with squeezing [16,17] and multipartite entanglement [18,19]. Based on this, we propose the amount of squeezing generated as an application-tailored performance benchmark of QAOA, which is able to capture the depth dependency of QAOA better than quantum volume [20–22], and can be used to detect errors. Our work thus further strengthens the intimate links between quantum metrology and quantum information processing [23–26]. Moreover, we show that warm-starting the optimization of a weighted MaxCut problem with a squeezed state can provide enhanced performance. We also discuss the parameter regimes, compared for different platforms, where a metrological task using a mulitparty-entangled squeezed state generated through QAOA could become advantageous over fast repetitions with simple unsqueezed states.

In the rest of this paper, we first provide some background in quantum optimization and spin squeezing (Sec. II). Then, QAOA is formally connected to the generation of entangled squeezed states (Sec. III), which was subsequently demonstrated numerically. Based on squeezing, then we develop a benchmark tailored for QAOA (Sec. IV), and assess the ability of superconducting qubits to run QAOA on fully connected problems while simultaneously creating Dicke states and estimate the number of entangled particles (Sec. IV C). Finally, we extend this connection for application in metrology and quantum optimization (Sec. V). In the Appendixes, we describe why squeezed states are entangled (Appendix A), define and connect multipartite entanglement to quantum
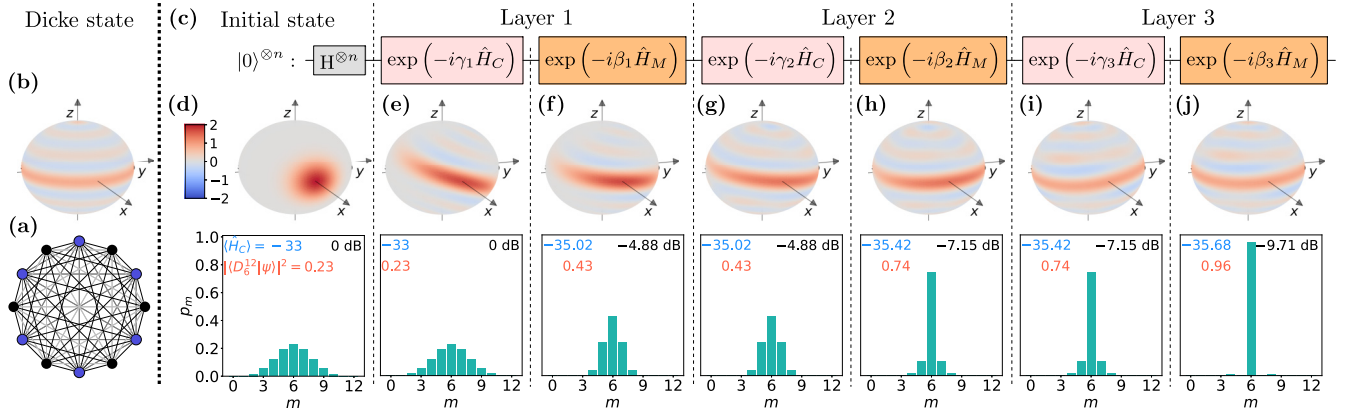
*gopal.santra@kip.uni-heidelberg.de

FIG. 1. Metrologically useful squeezing generated by a depth-three QAOA for the MaxCut problem in a complete graph of 12 nodes. (a) Fully connected unweighted graph with the nodes and edges colored according to one of the 924 possible maximum cut configurations. (b) Wigner quasiprobability distribution of the symmetric Dicke state D_6^{12}, an idealized example of a squeezed state and the target for our QAOA. (c) Circuit representation of QAOA with alternating application of cost function and mixer Hamiltonian. The Bloch spheres and histograms from (d) to (j) show the state after the corresponding gate in the optimized QAOA circuit with (γ_i, β_i) given by (0.199, 0.127), (0.306, 0.087), and (4.592, 1.518) for $i = 1$, 2, and 3, respectively. Negativity in the Wigner distribution indicates that the states are non-Gaussian [27]. The squeezing (in black), energy expectation $\langle \hat{H}_C \rangle$ (in blue), and overlap probability density $|\langle D_6^{12}|\psi\rangle|^2$ with the target Dicke state (in orange) are shown inside each histogram.

Fisher information and squeezing (Appendix B), explain the discontinuities observed in the benchmark in Fig. 3(b) (Appendix C), discuss the details of the optimization method used to obtain the parameters $\{\gamma, \beta\}$ (Appendix D), give details of the *ibmq_mumbai* (Appendix E), discuss metrological gain in different hardware (Appendix F), explain why increasing the duration of $\hat{H}_C$ is not helpful compared to the alternating layers in QAOA (Appendix G), discuss the advantages of using multiple layers of QAOA (Appendix H), and describe the complex energy landscape for an instance of MaxCut problem of a random graph of ten vertices (Appendix I).

II. BACKGROUND

In this section, we introduce QAOA for optimization problems such as MaxCut (Sec. II A), and describe how spin squeezing is generated in collective-spin observables (Sec. II B).

A. Combinatorial optimization on quantum computers

Universal quantum computers can address hard classical problems such as quadratic unconstrained binary optimization (QUBO), which is defined through

$$\min_{x \in \{0,1\}^n} x^T \Sigma x \quad \text{with } \Sigma \in \mathbb{R}^{n \times n}. \tag{1}$$

In QAOA, the binary variables x_i are mapped to qubits through $x_i = (1 - z_i)/2 \rightarrow (1 - \hat{Z}_i)/2$, where $\hat{Z}_i$ is a Pauli spin operator with eigenstates $|0\rangle$ and $|1\rangle$. The result is an Ising Hamiltonian $\hat{H}_C$ whose ground state is the solution to Eq. (1) [4]. The standard QAOA then applies p layers of the unitaries $\exp(-i\beta_k \hat{H}_M) \exp(-i\gamma_k \hat{H}_C)$, with $k = 1, \ldots, p$, to the ground state of a mixer Hamiltonian $\hat{H}_M$, such as $-\sum_i \hat{X}_i$ where $\hat{X}_i$ is a Pauli operator, to create the trial state $|\psi(\boldsymbol{\beta}, \boldsymbol{\gamma})\rangle$. A classical optimizer seeks the $\boldsymbol{\beta} = (\beta_1, \ldots, \beta_p)$ and $\boldsymbol{\gamma} = (\gamma_1, \ldots, \gamma_p)$

that minimize the energy $\langle \psi(\boldsymbol{\beta}, \boldsymbol{\gamma})|\hat{H}_C|\psi(\boldsymbol{\beta}, \boldsymbol{\gamma})\rangle$, which is measured in the quantum processor.

As an example problem, MaxCut aims at bipartitioning the set of nodes V in a graph $G(V, E)$ such that the sum of the weights $\omega_{i,j}$ of the edges $(i, j) \in E$ traversed by the cut is maximum, i.e.,

$$\max_{z \in \{-1,1\}^n} \frac{1}{2} \sum_{(i,j) \in E} \omega_{i,j}(1 - z_i z_j). \tag{2}$$

Consider the problem instance with $\omega_{i,j} = 1, \forall (i, j)$, i.e., an unweighted fully connected graph labeled $\mathcal{G}_n$ [see Fig. 1(b)]. Dividing V into two sets of size as equal as possible creates a maximum cut.

B. Squeezing

Squeezed states are entangled states with a reduced variance of one observable at the cost of an increased variance in noncommuting observables. A large body of experimental work exists addressing the generation of squeezing in various platforms [25,28–32]. Squeezing can also detect multipartite entanglement among qubits [33–37].

In our setting, we are interested in squeezing within an ensemble of n qubits (whose symmetric subspace can be seen as a qudit with length $\ell = \frac{n}{2}$). Consider a coherent state, such as the collective superposition $|+\rangle^{\otimes n}$, where $|+\rangle = (|0\rangle + |1\rangle)/\sqrt{2}$. This state has a variance of $\sigma_{\text{css}}^2 = \frac{n}{4}$, commonly called the shot noise, in the collective observable $\hat{L}_z = \frac{1}{2} \sum_{i=1}^n \hat{Z}_i$. By evolving $|+\rangle^{\otimes n}$, e.g., under the nonlinear one-axis-twisting (OAT) operator $\hat{L}_z^2 = \frac{1}{4}(n + \sum_{i \neq j} \hat{Z}_i \hat{Z}_j)$, the state is stretched over the collective Bloch sphere. The direction with reduced variance can be transferred to the z coordinate by rotating the state around the x axis with $\hat{L}_x = \frac{1}{2} \sum_{i=1}^n \hat{X}_i$ [16,30,38]. The resulting n-particle state is called number squeezed along z when the observed variance

is below σ_{css}^2, i.e., if the squeezing parameter

$$\mathcal{S}\,[\mathrm{dB}] = 10 \log_{10}\left(\frac{\mathrm{Var}(\hat{L}_z)}{\sigma_{\mathrm{css}}^2}\right) \tag{3}$$

is negative [16,17].

III. CONNECTING SQUEEZING TO QAOA

In a quantum circuit representation, the steps described above for the generation of squeezed states coincide with a single-layer QAOA sequence [see Fig. 1(c)]:

(i) The application of Hadamard gates to $|0\rangle^{\otimes n}$ initializes the system in $|+\rangle^{\otimes n}$, the ground state of the mixer Hamiltonian $\hat{H}_M$.

(ii) The evolution under the OAT operator corresponds to applying the unitary $\exp(-i\gamma_1\hat{H}_C)$ with the cost function $\hat{H}_C \propto \hat{L}_z^2$. On the qubit level, this corresponds to controlled-z gates generated by $\hat{Z}_i\hat{Z}_j$ between all qubits i and j.

(iii) The rotation around the x axis to reveal the squeezing corresponds to the unitary $\exp(-i\beta_1\hat{H}_M)$, i.e., an application of the mixer.

Interestingly, the cost function $\hat{H}_C \propto \hat{L}_z^2$ is a special instance of the MaxCut problem [Eq. (2)]. For even n, the set of all maximum cuts corresponds to the symmetric Dicke state [15]

$$D_k^n = \binom{n}{k}^{-1/2}\sum_i P_i(|1\rangle^{\otimes k} \otimes |0\rangle^{\otimes(n-k)}), \tag{4}$$

with $k = \frac{n}{2}$. Here, $P_i(\cdot)$ denotes a permutation of all states with k particles in $|1\rangle$ and $n - k$ particles in $|0\rangle$. For odd n, the set of all maximum cuts corresponds to $(D_{\lfloor n/2\rfloor}^n + D_{\lceil n/2\rceil}^n)/\sqrt{2}$. These states are maximally squeezed along z and are the most useful for metrological applications [10]. The QAOA cost function Hamiltonian to minimize in this problem is $\hat{H}_C = \frac{1}{2}\sum_{i<j}(\hat{Z}_i\hat{Z}_j - 1) = \hat{L}_z^2 - \frac{n^2}{4}\mathbb{I}$. Therefore, QAOA tasked to find the maximum cut of a fully connected unweighted graph will maximize the squeezing. This relation thus translates analog metrological protocols [30] to a digital quantum processor. In addition, by formulating the constraints that an arbitrary Dicke state D_k^n imposes on the spins as a QUBO, we can generate D_k^n for arbitrary k (see Sec. V A).

A. QAOA as generator of squeezing

To illustrate the connection between QAOA and squeezing, we numerically simulate a system with $n = 12$ qubits and follow the usual QAOA protocol, using $\hat{H}_C = \hat{L}_z^2 - \frac{n^2}{4}\mathbb{I}$, $\hat{H}_M = -2\hat{L}_x$, and $p = 3$ (Appendix D). We depict the generated collective qudit state using the Wigner quasiprobability distribution as well as the probability distribution over the spin eigenvalues $\{m = \langle\hat{L}_z\rangle + \frac{n}{2}\}$ at each step [see Figs. 1(d)–1(j)]. Each application of $\hat{H}_C$ stretches the Wigner distribution, making it resemble an ellipse with the major axis tilted with respect to the equatorial plane of the qudit Bloch sphere. As $[\hat{H}_C, \hat{L}_z] = 0$, this operation does not alter the distribution of $\langle\hat{L}_z\rangle$. Next, the mixer operator rotates the Wigner distribution back towards the equator, thereby transferring the squeezing to the operator $\hat{L}_z$. After three layers, the final state has an overlap with the symmetric Dicke state of 96% and the

squeezing number reaches $\mathcal{S} = -9.71$ dB. Crucially, noiseless QAOA with less layers produces less squeezing (e.g., see depth-one QAOA; Appendix G).

B. Multipartite entanglement

The squeezing in collective spin observables can further be related to entanglement. We employ three different criteria:

(E1) If $\frac{n}{4} > \langle\hat{L}_z^2\rangle$, the state violates a bound on separable states [37]. Any squeezed state $(\mathrm{Var}(\hat{L}_z) < \frac{n}{4})$ at the equator $(\langle\hat{L}_z\rangle = 0)$ is witnessed as entangled by this criterion (Appendix A). Here, $\langle\hat{L}_z^2\rangle = 0.32 < \frac{n}{4} = 3$, which is close to the minimal value of 0 achieved by the Dicke state.

(E2) If the quantum Fisher information for a pure state ψ, $F_Q[\psi, \mathcal{O}] = 4\mathrm{Var}(\mathcal{O})$, is larger than $(sk^2 + r^2)$, where $s = \lfloor n/k\rfloor$ denotes the integer division of n by k, and r is the remainder, at least $(k + 1)$ particles are entangled [18,19]. Here, $F_Q[\psi, \hat{L}_y] = 84.48$ and the final state has multipartite entanglement between at least 9 out of 12 particles (Appendix B).

(E3) Specifically for Gaussian states, one can approximately estimate the number of entangled particles k assuming the identity $F_Q/n \simeq \sigma_{\mathrm{css}}^2/\mathrm{Var}(\hat{L}_z)$ [30] (Appendix B), which here yields $k = 11$. We will use this estimate below in the hardware results where direct access to F_Q is not possible (Sec. IV C).

C. Metrology

Increasing the number of measurements also reduces the variance of a phase estimation. It is thus important to analyze when QAOA-prepared squeezed states can be convenient for a metrological task, as compared to simply repeating various shots with an unsqueezed coherent time. With that motivation, we study the time taken to measure a phase θ with the coherent spin state (CSS) versus QAOA-generated Dicke states within different hardware architectures (but without an attempt at comparing the different architectures to each other, which often have different aims and boundary conditions that are difficult to compare on an even footing). The coherent state is easily prepared by a single rotation around the y axis. It has no entanglement, and m measurements of the phase θ have a variance bound by $\Delta^2\theta \geqslant 1/(mN)$. By contrast, a QAOA-prepared state with F_Q above the $(k + 1)$-partite entangled limit takes more time to prepare than the CSS, but it requires a smaller number of measurements to reach the same variance since $\Delta^2\theta \geqslant 1/(mkN)$ is lowered by a factor of $1/k$ [19].

One may then wonder whether, in a practical application, the improved precision can offset the larger preparation time. Crucially, the optimization cost of QAOA can be ignored in these considerations since the optimal $\boldsymbol{\gamma}$ and $\boldsymbol{\beta}$ parameters are reusable across different measurements and experiments. We therefore compute the duration of a single measurement repetition t_{repet}, which is the sum of the duration of the gates in the circuit to prepare the state t_{gates} and the readout time including the reset of the measurement apparatus t_{rr}, i.e., $t_{\mathrm{repet}} = t_{\mathrm{gates}} + t_{\mathrm{rr}}$. The gate duration for the coherent spin state $t_{\mathrm{gate}}^{\mathrm{CSS}}$ is the duration of a single-qubit gate, while the QAOA protocol requires two-qubit gates, whose number can depend

TABLE I. Duration of key operations presented as orders of magnitude only. The entangling operations for the transmons, trapped ions, and cold atoms are the two-qubit CNOT gate, the Mølmer-Sørensen gate, and the one-axis twisting Hamiltonian, respectively.

Platform	Single-qubit	Entanglement	Readout and reset t_{rr}
Transmons	10 ns [44]	100 ns [21]	100 μs [45]
Trapped ions [46]	15 μs	200 μs	300 μs +5 ms [47]
Cold atoms (BEC)		10 ms [30]	1 s

on the available universal gate set and the hardware connectivity.

The QAOA-generated states are advantageous when the time $t^{QAOA} = t_{repet}^{QAOA} m_{QAOA}$ to achieve a certain precision is smaller than the time $t^{CSS} = t_{repet}^{CSS} m_{CSS}$ to achieve the same precision with coherent states. If the QAOA-prepared state achieves $F_Q = kN$, we have for equal precision $m_{QAOA}k = m_{CSS}$; i.e., the QAOA-prepared states are advantageous if

$$t_{gates}^{QAOA} + t_{rr} < k\left(t_{gates}^{CSS} + t_{rr}\right). \tag{5}$$

a. Superconducting qubits. The duration of a QAOA layer is impacted by the qubit connectivity. Each QAOA layer on N linearly connected superconducting qubits requires $3(N - 2)$ layers of simultaneously executable controlled-NOT (CNOT) gates which includes SWAP gates [39]. Under the assumption that QAOA can create $(k + 1)$-partite entanglement in $p = \log_2(k)$ layers [40], the duration $t_{gates}^{QAOA} = 3(N - 2)\log_2(k)t_{cx}$ with t_{cx} the duration of a CNOT gate. Here, we neglected the duration of single-qubit gates. With $k = N$, Eq. (5) yields

$$3(N - 2)\log_2(N)t_{cx} + t_{rr} \lesssim Nt_{rr} \tag{6}$$

which, for large N and the durations in Table I, amounts to

$$N \lesssim 2^{t_{rr}/(3t_{cx})} = 2^{1000/3}. \tag{7}$$

Although the linear layout of the hardware poses a limit on when QAOA-generated states remain useful, this limit is extremely high. Assuming noisy hardware achieves only a finite k, one has

$$(N - 2)\log_2 N < (k - 1)t_{rr}/(3t_{cx}). \tag{8}$$

For $k = 2$, e.g., the QAOA-generated states would remain advantageous up to about 60 qubits arranged in a linear chain, which lies at the size limit of the current hardware. These numbers are conservative estimates that can be significantly increased by improved noise resilience and higher hardware connectivity.

b. Trapped-ion qubits. Large multipartite entangled states of trapped ions can be generated by a single application of the Mølmer-Sørensen (MS) gate [41,42], where interaction strength among all qubit pairs is equal [43]. Therefore, if we neglect the duration of single-qubit gates, t_{gates}^{QAOA} only depends on the number of QAOA layers $p = \log_2(k)$, and $t_{gates}^{QAOA} = \log_2(k)t_{ms}$ with t_{ms} being the duration of a MS gate. Following Table I, QAOA-generated $(k + 1)$-partite entangled states are therefore advantageous when

$$\log_2(k)t_{ms} \lesssim (k - 1)t_{rr} \Rightarrow k^{\frac{1}{k-1}} \lesssim 2^{t_{rr}/t_{rm}} = 2^{25}. \tag{9}$$

Since $k^{1/(k-1)}$ is a decreasing function, QAOA-generated states are always advantageous in trapped-ion setups.

c. Cold atoms. We now consider cold atoms in Bose-Einstein condensates which can, e.g., manipulate states with of the order of 400 atoms [30]. Following QAOA, we assume that $\log_2(k)$ layers of the one-axis-twisting Hamiltonian interleaved with x rotations can generate $(k + 1)$-partite entanglement. The squeezed state is thus created in a time $t_{gates}^{QAOA} = \log_2(k)t_{OAT}$. We neglect the duration of x and y rotations. Equation (5) implies $\log_2(k)t_{OAT} < (k - 1)t_{rr}$, showing that given a Bose-condensed atom cloud of fixed size it is always favorable to create spin-squeezed states for metrology since $t_{OAT} \ll t_{rr}$ (see Table I).

IV. QAOA-TAILORED HARDWARE BENCHMARKS

The performance of quantum computing hardware is often measured by metrics such as randomized benchmarking [48–50] and quantum process tomography [51,52], which focus on gates acting on typically one to two qubits, while quantum volume (QV) (Sec. IV A) is designed to measure the performance of a quantum computer as a whole [20–22]. For certain applications, these are complemented by specifically designed benchmarks, e.g., for quantum chemistry [53], generative modeling [54,55], variational quantum factoring [56], Fermi-Hubbard models [57], and spin Hamiltonians [58]. It is of particular interest to identify such application-tailored benchmarks also for variational algorithms, as these employ highly structured circuits. This necessity is well illustrated by considering the QV: the circuit complexity of a 2^n QV system is equivalent to a $p = 2$ QAOA running on n linearly connected qubits.

A. Quantum volume

A processor with a quantum volume of $QV = 2^n$ can reliably, as defined by the generation of heavy output bit-strings, execute circuits that apply n layers of SU(4) gates on random permutations of n qubits [20]. When transpiled to a line of n qubits, QV circuits result in n layers of SU(4) gates that have at most $\lfloor \frac{n}{2} \rfloor$ individual SU(4) gates simultaneously executed on the qubits [21]. In between these SU(4) layers, there are at most $\lfloor \frac{n}{2} \rfloor$ SWAP gates (see Fig. 2). Furthermore, each SU(4) and SWAP gate require at most and exactly three CNOT gates, respectively [59]. Under these conditions, the total number of CNOT gates is at most

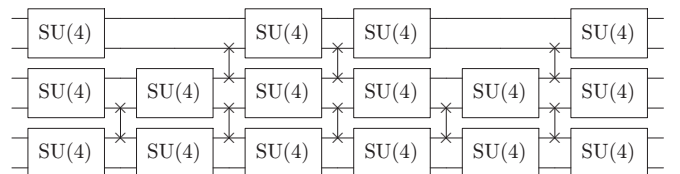$$3n \left\lfloor \frac{n}{2} \right\rfloor + 3(n - 1) \left\lfloor \frac{n}{2} \right\rfloor, \tag{10}$$

FIG. 2. Example of a six-qubit quantum volume circuit as presented in Ref. [21], which shows the layers of SU(4) and SWAP gates.

which approaches $3n^2$ as n becomes large. By comparison, the cost operator of QAOA circuits of complete graphs transpiled to a line requires exactly $\frac{3}{2}n(n-1) - n + 1$ CNOT gates, approaching $3n^2/2$ for large n. This suggests that a 2^n quantum volume is a good performance indicator for a depth $p = 2$ QAOA on n qubits. Importantly, this comparison is only possible as long as the QAOA circuit is executed using the same error mitigation and transpilation methods as those employed to measure QV [22]. However, QV fails to capture the depth dependency p of QAOA. The benchmark that we develop overcomes this limitation as the QAOA depth should be chosen such that the measured squeezing is maximum. This also provides the maximum p for which it makes sense to run QAOA on the benchmarked noisy hardware.

B. Proposed benchmark

As the above section shows, QV fails to properly capture the dependency on p as QAOA circuits on complete graphs are deeper than their width. As Ref. [60] shows using entropic inequalities, if the circuit is too deep a classical computer can sample in polynomial time from a Gibbs state while achieving the same energy as the noisy quantum computer. That bound is based on the fidelity of layers of gates, which is, however, often overestimated when built from fidelities of gates benchmarked in isolation, e.g., due to cross-talk [39].

Since the solution to the MaxCut problem on the fully connected unweighted graph $\mathcal{G}_n$ is known, we propose squeezing as a good hardware benchmark for QAOA to complement other performance metrics. For our proposed benchmark, we first label the quantum numbers of $\hat{L}_z + \frac{n}{2}$ by $m \in \{0, 1, \ldots, 2\ell\}$, which correspond to cuts of size $c(m) = m(n - m)$ on $\mathcal{G}_n$. We relate squeezing to a QAOA performance metric through the following question: Given the squeezing $\mathcal{S}$ in the trial state, what is the probability $P_\alpha(n, \mathcal{S})$ of sampling a cut with size $c(m)$ greater than a given α fraction of the maximum cut size $c_{max} = n^2/4$?

Here, α can be seen as an approximation ratio. By definition, cuts with $c(m) > \alpha c_{max}$ must satisfy $m_-(\alpha) < m < m_+(\alpha)$ for even n, where $m_\pm(\alpha) = \frac{n}{2}(1 \pm \sqrt{1 - \alpha})$. Under a QAOA trial state $|\psi(\boldsymbol{\beta}, \boldsymbol{\gamma})\rangle$ with a distribution p_m over m [see Fig. 3(a)], the probability to sample cuts larger than αc_{max} is thus

$$P_\alpha(n) = \sum_{m = \lceil m_-(\alpha) \rceil}^{\lfloor m_+(\alpha) \rfloor} p_m. \tag{11}$$

We now make the simplifying assumption that the distribution p_m is a Gaussian $\mathcal{N}(\frac{n}{2}, \sigma)$, where the standard deviation σ—the only free variable for fixed n—is, by definition, in one-to-one correspondence to the squeezing $\mathcal{S} = 10 \log_{10}(4\sigma^2/n)$. In summary, the benchmark (i) relates squeezing to the probability of sampling good solutions, a QAOA performance metric, (ii) captures the ability of QAOA to create entangled states (Sec. III B), and (iii) is as susceptible to hardware noise as other fully connected QAOA circuits (Sec. IV E).

We illustrate the benchmark by numerically computing $P_\alpha(n, \mathcal{S})$ as a function of n and the squeezing $\mathcal{S}$ in the
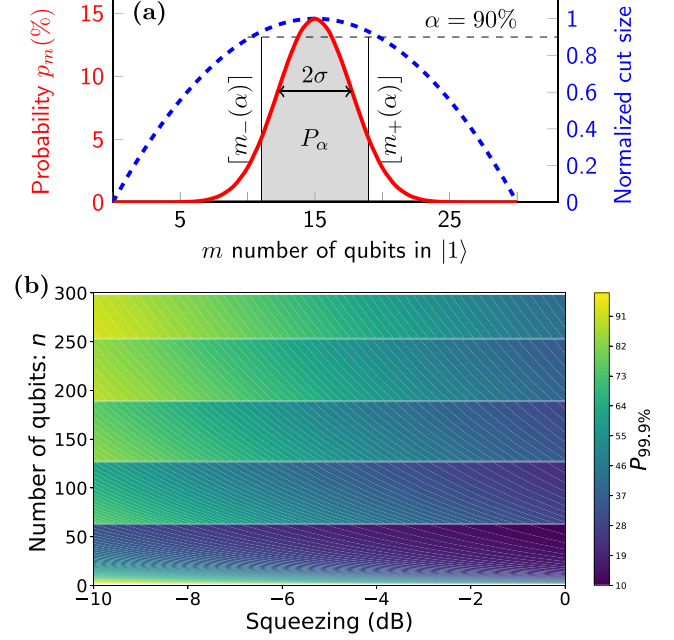

FIG. 3. Benchmarking QAOA with squeezing. (a) Probability distribution (p_m, red solid line) and normalized cut size (c_m/c_{max}, blue dashed line) simultaneously plotted against $m = \langle \hat{L}_z \rangle + \frac{n}{2}$ for $n = 30$. States with normalized cut size more than α lie in $m \in [\lceil m_-(\alpha) \rceil, \lfloor m_+(\alpha) \rfloor]$. These yield the shaded area under the probability p_m, which is the figure of merit P_α defined in Eq. (11). (b) P_α showing how the probability of sampling high-value cuts changes with the squeezing $\mathcal{S}$ and the number of qubits, n, calculated using trial Gaussian distributions.

Gaussian distribution $p_m(\mathcal{S})$. Since the ground state of $\mathcal{G}_n$ is highly degenerate, we select a high value of α, e.g., 99.9%. At fixed n, an increased squeezing (more negative) increases P_α [see Fig. 3(b)], as cuts with a larger size receive more weight. In addition, P_α has discontinuous jumps at $n_{dis.}$, where $z = \lfloor \frac{n_{dis.}}{2} \sqrt{1 - \alpha} \rfloor \in \mathbb{Z}^+$ (Appendix C). In between discontinuities, P_α diminishes with increasing n because σ increases $\propto \sqrt{n}$ for fixed $\mathcal{S}$, which reduces the weight attributed to high-value cuts.

C. Benchmarking superconducting qubits

We now evaluate the benchmark on gate-based superconducting transmon qubits [61]. We measure the squeezing on the IBM Quantum system *ibmq_mumbai* using QISKIT [62] for four, six, and eight qubits (Appendix E). Since the chosen qubits have a linear connectivity, we use a line swap strategy [39,63] to create the all-to-all qubit connectivity required by the squeezing circuit, shown in Fig. 4(a) for $p = 1$. This circuit is then transpiled to the cross-resonance-based hardware [64,65] employing a pulse-efficient strategy instead of a CNOT decomposition [66] using QISKIT PULSE [67]. The optimal value of the variational parameter γ is found with a noiseless simulation for each n. We use readout error mitigation [68,69], which on average improves the best measured squeezing by -0.7 ± 0.1 dB averaged over all three $n \in \{4, 6, 8\}$. At depth one, a sweep of the tomography angle β_1 reveals a squeezing of -4.80, -4.18, and -4.02 dB whereas noiseless simula-
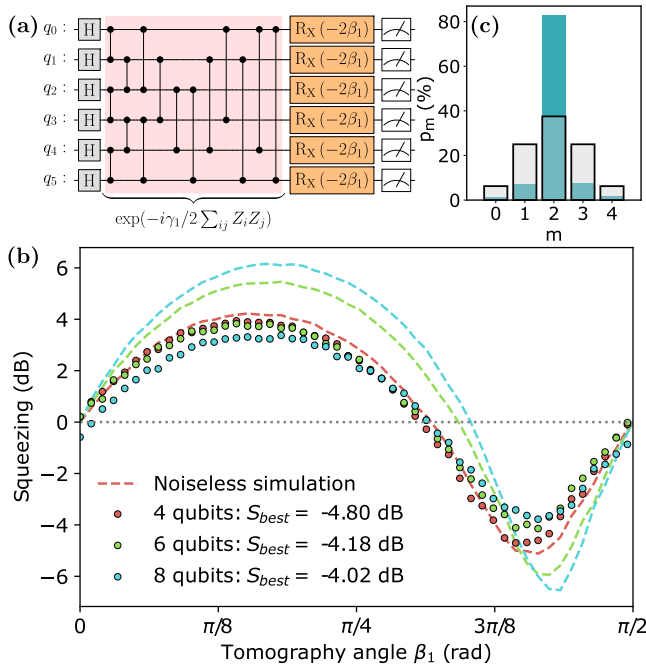
FIG. 4. Squeezed states generated on superconducting qubits. (a) A quantum circuit implementing a single QAOA layer for the MaxCut problem on a six-qubit system, producing a state with a reduced variance along the z axis. (b) Squeezing measured with the quantum circuit in (a). The dashed lines show a noiseless QASM simulation. (c) The p_m distribution of the four-qubit state with -5.96 dB squeezing generated by a depth-two QAOA with optimal parameters $\gamma_1 = 0.918$, $\gamma_2 = -0.257$, $\beta_1 = -0.711$, and $\beta_2 = -2.175$. The gray histogram shows the state $(H|0\rangle)^{\otimes n}$.

tions reach -5.14, -5.90, and -6.56 dB for $n = 4$, 6, and 8, respectively. These metrological gains are comparable to prior works in trapped ions [42,70–74] (Appendix F). Given the measured squeezing, we compute a $P_{99.9\%}(n, \mathcal{S})$ of 61.5%, 49.1%, and 42.6%, respectively. Furthermore, we run a depth-two QAOA on the fully connected four-qubit graph to create a state with a -5.96 dB squeezing [see Fig. 4(c)], which results in $P_{99.9\%}(4, -5.96) = 68.2\%$. These results indicate that the potential to generate squeezing in a four-qubit system is limited by the variational form at depth one. By contrast, in systems with six and eight qubits, the squeezing generated in practice is limited by the large number of CNOT gates at depth one (40 and 77, respectively). Criterion (E1) witnesses the generated states in both simulation and hardware as entangled [see Fig. 5(a)]. In a noiseless simulation of a depth-one QAOA of system sizes $n = 4, 6, 8$, criterion (E2) witnesses at least four-, four-, and five-qubit entanglement, respectively. In the noisy hardware implementation, estimate (E3) suggests these numbers to still reach 4, 3, and 3, respectively.

D. Squeezing as a good benchmark for arbitrary QUBO problem

From a hardware perspective, although $\mathcal{G}_n$ is a specific problem, its QAOA circuit is representative of the noise of an arbitrary fully connected QUBO problem since the gates constituting a generic cost function $\exp(-i\gamma_k \hat{H}_C)$ can
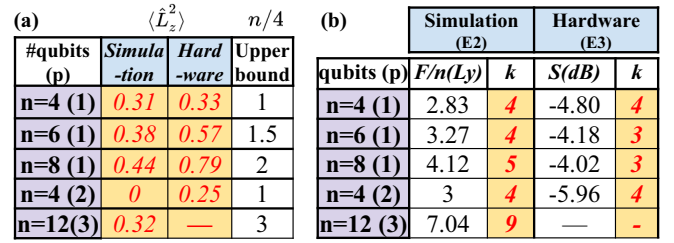

FIG. 5. Entanglement from squeezing and quantum Fisher information. (a) The values of $\langle \hat{L}_z^2 \rangle$ (E1) obtained in simulation and hardware are close to zero, indicating that the states are in the vicinity of entangled Dicke states. (b) Number of entangled particles k calculated from $F_Q[\hat{L}_y]$ (E2) in simulation, and estimated for hardware using (E3).

be implemented with virtual Z rotations and CNOT gates [75]. Indeed, the difference between the pulse schedules only amounts to phase changes, indicated by circular arrows in Fig. 6(c). The duration of the QAOA pulse schedule and the absolute amplitude of the pulses are thus independent of the variables Σ in the QUBO [see Eq. (1)] and the variational parameters $\boldsymbol{\gamma}$ and $\boldsymbol{\beta}$ [compare Figs. 6(b) and 6(c)]. Therefore, much like quantum volume, the hardware benchmark based on squeezing captures effects such as limited qubit connectivity, unitary gate errors, decoherence, and cross-talk. Furthermore, from a hardware perspective, the squeezing circuit is also the hardest to implement since QUBOs
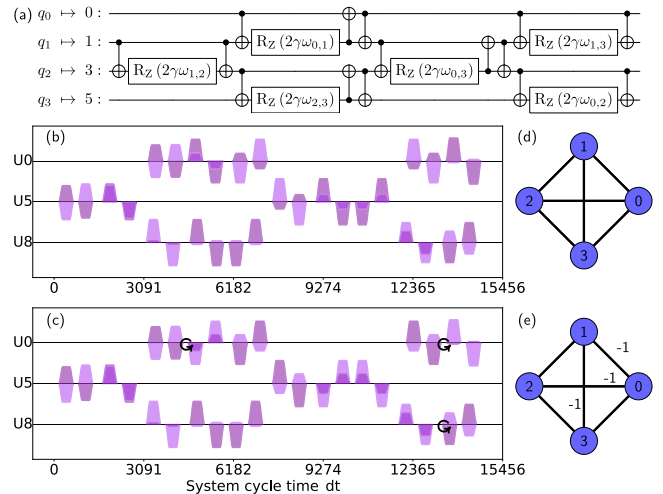

FIG. 6. Cross-resonance pulse schedules of the squeezing circuit and an arbitrary QUBO. (a) Quantum circuit of a general four-qubit fully connected cost operator $e^{-i\gamma\hat{H}_C}$ transpiled to qubits 0, 1, 3, and 5 of *ibm_lagos*. (b) Pulse schedule of the cost operator used to generate the symmetric Dicke state, i.e., $\omega_{i,j} = 1 \, \forall i, j$. (c) Pulse schedule of a MaxCut instance with edge weights $\omega_{0,1} = \omega_{0,2} = \omega_{1,3} = -1$ and $\omega_{0,3} = \omega_{1,2} = \omega_{2,3} = 1$. The circular arrows show where the phase shifts differ from the pulse schedule in (b). [(d) and (e)] MaxCut graph corresponding to the pulse schedules in (b) and (c), respectively. The duration of a single sample of the arbitrary waveform generators is d$t = 0.222$ ns. The light and dark pulses show the in-phase and quadrature of each complex amplitude pulse applied to control channels U0, U5, and U8 of *ibm_lagos*.
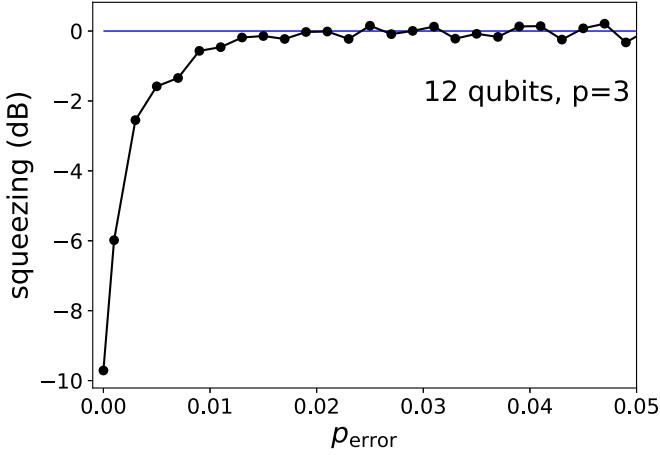
FIG. 7. Squeezing as a function of the strength of gate noise modeled as bit-flip errors. A bit-flip error is added to every CNOT gate by two-qubit Pauli channels, $\mathcal{P}_2 = \mathcal{P}_1 \otimes \mathcal{P}_1$, where $\mathcal{P}_1 = \sqrt{p_{\text{error}}}X + \sqrt{1 - p_{\text{error}}}I$. The squeezing approaches zero as gate errors increase, showing the validity of squeezing as an application-tailored hardware benchmark.

that are not fully connected, i.e., $\exists (i, j) \,|\, \Sigma_{i,j} = 0$, require less pulses.

E. Error detection by spin squeezing

As undesired processes destroy fragile quantum superpositions, the degree of squeezing is sensitive to the noise levels of the quantum device. To illustrate this, we run our depth-three QAOA example of Fig. 1 on a noisy simulator. After each CNOT gate, we include a Pauli bit-flip error with strength p_{error}. We observe that the squeezing rapidly decays towards zero as p_{error} increases, resulting in a nonsqueezed state (see Fig. 7). This simple simulation demonstrates that gate errors destroy the fragile correlations needed to create a squeezed state. Conversely, the ability (or inability) to realize squeezing through QAOA can be used as a tool to estimate the errors in a circuit experiment.

V. EXTENSION

In this section, we extend the connection between QAOA and metrology to create arbitrary Dicke states and warm-starting QAOA with partially squeezed states for random MaxCut problems.

A. Creating arbitrary Dicke states

We can create arbitrary Dicke states [Eq. (4)] by minimizing a QUBO cost function with QAOA. Let $|x_{n-1} \cdots x_0\rangle$ be a basis state in which qubit i is in state $x_i \in \{0, 1\}$. Each basis state in D_k^n satisfies the equation $\sum_{i=0}^{n-1} x_i = k$, which is a constraint on the binary variables x_i. We express this constraint as the QUBO problem

$$\min_{x \in \{0,1\}^n} \left(k - \sum_{i=0}^{n-1} x_i \right)^2. \quad (12)$$

TABLE II. The parameters (γ_i, β_i) of an optimized depth-three QAOA circuit to create $k = 1, 2, 3, 4, 5$ Dicke states.

No. spin up, k	γ_1	β_1	γ_2	β_2	γ_3	β_3
1	0.101	0.903	0.317	1.324	1.506	−0.155
2	0.093	1.106	0.427	1.409	1.457	−0.068
3	0.149	1.205	1.645	1.576	0.472	−0.076
4	0.111	1.220	0.441	1.690	1.028	0.062
5	0.231	1.340	1.643	1.500	1.774	0.004

The solution to this optimization problem is a superposition of all basis states with k qubits in the excited state, i.e., D_k^n. We apply the change of variables $x_i = (z_i + 1)/2$ to rewrite $(k - \sum_i x_i)^2$ as

$$k^2 - kn + \frac{n}{4}(n + 1) + \left(\frac{n}{2} - k \right) \sum_{i=0}^{n-1} z_i + \frac{1}{2} \sum_{i<j} z_i z_j. \quad (13)$$

After promoting each z_i variable to a Pauli spin operator $\hat{Z}_i$, Eq. (13) yields a cost Hamiltonian to minimize

$$\hat{H}_C = \left(\frac{n}{2} - k \right) \sum_{i=0}^{n-1} \hat{Z}_i + \frac{1}{2} \sum_{i<j} \hat{Z}_i \hat{Z}_j. \quad (14)$$

When $k = n/2$, we recover the MaxCut problem on the symmetric graph. For $k \neq n/2$, we have an extra term $(n/2 - k) \sum \hat{Z}_i$ that biases the total spin towards $\langle \hat{Z} \rangle = k$. The Hamiltonian in Eq. (14) can therefore be used to generate the Dicke state D_k^n with QAOA.

For $n = 12$ qubits, we use the cost Hamiltonian in Eq. (14) to simulate the generation of Dicke states with $k = 1, 2, 3, 4, 5$. With three QAOA layers, we obtain fidelities in excess of 80% (see Fig. 8). The corresponding QAOA parameters γ and β are shown in Table II.

B. Warm-starting QAOA with squeezed states

In this section, we explore how far the symmetric MaxCut problem that has a Dicke state as a ground state can help solve nontrivial MaxCut problems with asymmetric edge weights. We show how such squeezed states increase the likelihood of sampling good cuts on graphs with random edge weights. Each edge $\omega_{i,j}$ of a graph is sampled from a Gaussian distribution $\mathcal{N}(\mu, \epsilon)$ and then rounded to one decimal place to increase the separation in the cut values of the graph. We compare standard QAOA with p layers to a QAOA with $p_s + p$ layers in which the first p_s layers have fixed parameters to produce a squeezed state. Both methods, therefore, have $2p$ parameters that require optimization for each graph instance. For the second approach, in addition, $2p_s$ parameters are optimized once with the symmetric MaxCut problem as a target and are reused for different problem instances. For each $n \in \{4, 6, 8, 10, 12\}$, we sample 100 graph instances from $\mathcal{N}(\mu, \epsilon)$ for which we choose $\mu = 4$ and $\epsilon = 0.5$ and optimize the cut value for varying p. The resulting energy normalized to the minimum energy and averaged over the 100 graph realizations is used to compare both methods. To ensure that p layers always produce a result that is at least as good as the one for $p - 1$ layers, we
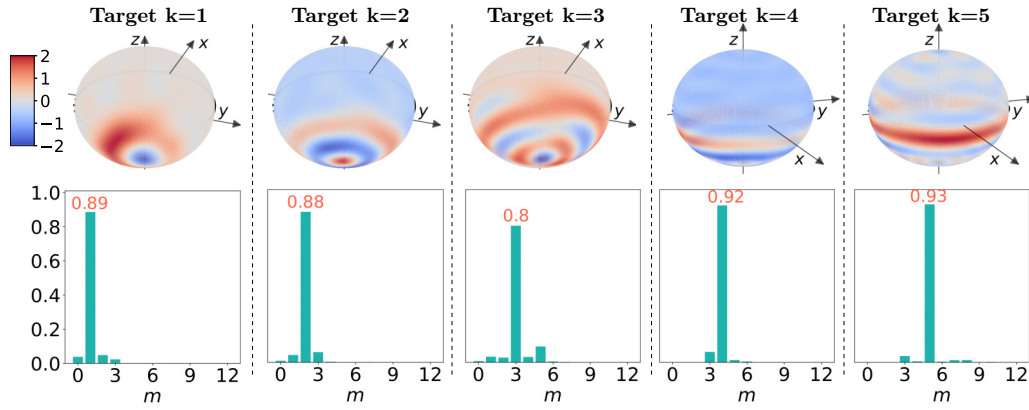
FIG. 8. Metrologically useful arbitrary Dicke states generated by a depth-three QAOA by minimizing the cost Hamiltonian in Eq. (14). The top panels show the Wigner quasiprobability distribution on the Bloch spheres. The bottom panels show the corresponding histograms of the total spin operator $\langle \hat{Z} \rangle = m$. The orange numbers in each histogram show the overlap probability density $|\langle D_k^{12} | \psi \rangle|^2$ with the target Dicke states.

bootstrap the optimization parameters. The initial guess of the parameters for layer p is based on the optimized parameters of layer $p-1$, i.e., $(\beta_1, \beta_2, \ldots, \beta_p, \gamma_1, \gamma_2, \ldots, \gamma_p)_{\text{initial}} = (\beta_1^{\text{opt}}, \beta_2^{\text{opt}}, \ldots, \beta_{p-1}^{\text{opt}}, 0, \gamma_1^{\text{opt}}, \gamma_2^{\text{opt}}, \ldots, \gamma_{p-1}^{\text{opt}}, 0)$.

QAOA initialized with squeezed states, shown as orange circles and green stars in Fig. 9, significantly improves the average energy when compared to QAOA initialized from an equal superposition, shown as blue triangles in Fig. 9. We observe little improvement in solution quality with increasing p. We attribute this to the complexity of the optimization landscape which has many local minima, even at depth one, due to the interference of the frequencies generated by the different edge weights (see Fig. 13). In the four-qubit case, the energy for $p \geqslant 3$ layers of both methods is comparable. As the system size is increased, we observe a greater advantage for QAOA initialized with a squeezed state. These results indicate that, when solving a family of problems, it may be advantageous to initialize QAOA with a state that corresponds to the average problem even when such a problem is trivial to solve.

VI. CONCLUSION

In summary, the generation of squeezed states that are useful for metrology can be cast as a MaxCut problem, which in turn can be addressed with variational algorithms. The procedure that we illustrated in the creation of a 12-qubit Dicke state can be implemented on universal quantum computing platforms, such as superconducting qubits or trapped ions, as well as on special purpose machines such as BECs trapped in optical tweezers [30]. Interestingly, an enhancement of squeezing within the multilayer QAOA protocol is not equivalent to simply applying the $\hat{L}_z^2$ operator for a longer period, as the mixer Hamiltonian periodically intervenes (Appendix H). Our results show how variational algorithms may generalize existing protocols and provide systematic guidance for the creation of highly squeezed states for metrology. By contrast to, e.g., Refs. [25,76–78], which use variational quantum algorithms with a hardware native *Ansatz* to enhance phase sensitivity, the QAOA approach

to create squeezing encapsulates the structure of the target state in the variational form which may reduce the number of parameters to optimize. In a similar vein, we foresee that custom states beyond Dicke states may be generated by QAOA if they can be cast as solutions of a combinatorial optimization problem. In addition, we suggested squeezing as a QAOA-specific hardware benchmark. This benchmark is both portable across hardware platforms and captures hardware-specific properties such as limited qubit connectivity and cross-talk.
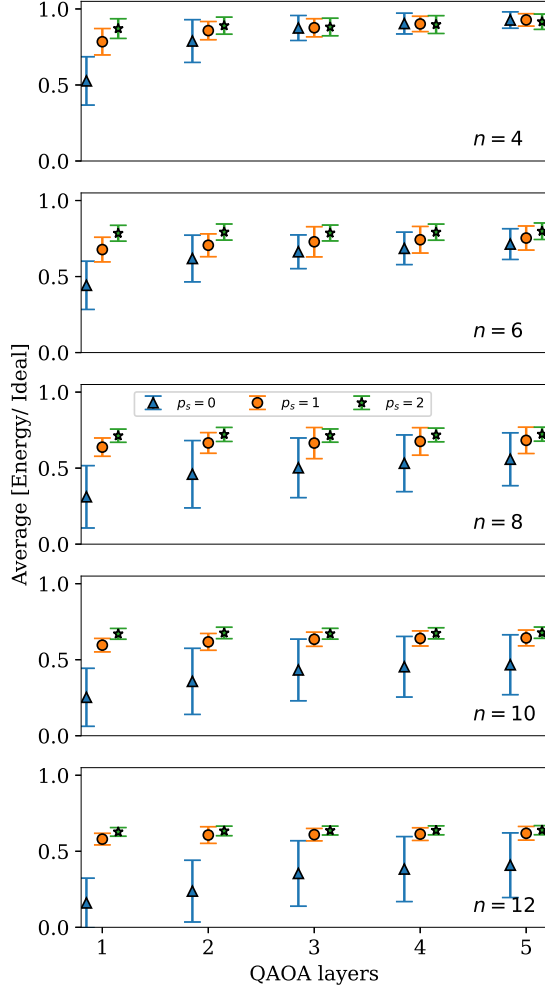
FIG. 9. Advantage of QAOA initialized with squeezed states. The blue triangles show standard QAOA initialized from a coherent spin state. The orange circles and green stars show QAOA initialized with a spin-squeezed state created with $p_s = 1$ and 2 QAOA layers, respectively. The x axis is the QAOA depth after the initial state and the y axis is the energy normalized to the ideal value. The markers and error bars indicate the average and variance of 100 graph instances drawn from $\mathcal{N}(4, 0.5)$ with different sizes $n = 4$ (top) to $n = 12$ (bottom). Squeezed initial states boost the average energy of the QAOA optimized state as shown by the orange and green markers having an energy that is closer to the ideal energy than the blue markers. The energy increases only modestly as p increases due to the complexity of the optimization landscape.

APPENDIX A: ENTANGLEMENT FROM SQUEEZING

Measurements of collective spin observables can reveal entanglement. In particular, separable states satisfy [37]

$$\langle \hat{L}_x^2 \rangle + \langle \hat{L}_y^2 \rangle \leqslant \frac{n}{2}\left(\frac{n}{2} + \frac{1}{2}\right) \Longleftrightarrow \frac{n}{4} \leqslant \langle \hat{L}_z^2 \rangle = \mathrm{Var}(\hat{L}_z).$$

(A1)

The second implication is reached using the identity $\langle \hat{L}^2 \rangle = \langle \hat{L}_x^2 \rangle + \langle \hat{L}_y^2 \rangle + \langle \hat{L}_z^2 \rangle = \frac{n}{2}(\frac{n}{2} + 1)$, and $\langle \hat{L}_z \rangle = 0$ for our target states. Any squeezed state defined through Eq. (3) violates the relation above and is thus entangled. Moreover, $\langle \hat{L}_x^2 \rangle +$
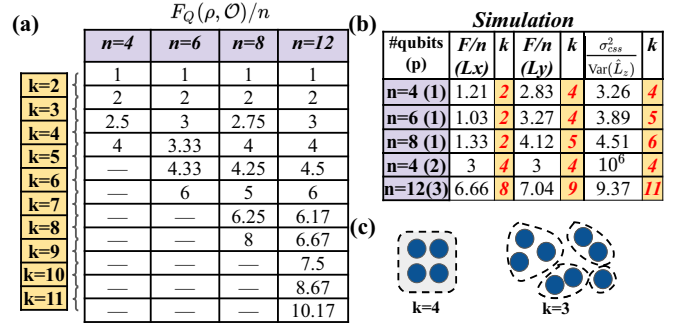

FIG. 10. Multipartite entanglement from quantum Fisher information and number squeezing. (a) F_Q witnessing k-partite entanglement for different n. (b) In the simulations, F_Q obtained with $\hat{L}_y$ is larger than $\hat{L}_x$. The numbers of entangled particles (k) estimated from squeezing ($\sigma_{\mathrm{css}}^2/\mathrm{Var}(\hat{L}_z) = 10^{-\mathcal{S}/10}$) are close to the numbers obtained from $F_Q[\hat{L}_y]$ for most cases. In a proper Dicke state as obtained with $n = 4 (p = 2)$, the $\mathrm{Var}(\hat{L}_z)$ becomes extremely small, leading to the very large value of $\sigma_{\mathrm{css}}^2/\mathrm{Var}(\hat{L}_z)$ seen in the fourth row. (c) Illustrative examples of k-partite entanglement as entanglement depth.

$\langle \hat{L}_y^2 \rangle$ reaches the maximum $\frac{n}{2}(\frac{n}{2} + 1)$ in the Dicke state [37], which is the same as having $\mathrm{Var}(\hat{L}_z) = 0$. In Fig. 5(a), we show how the obtained values of $\langle \hat{L}_z^2 \rangle$ are close to the minimum limit zero, revealing the existence of significant entanglement.

APPENDIX B: MULTIPARTITE ENTANGLEMENT, QUANTUM FISHER INFORMATION, AND SQUEEZING

A pure state of n qubits, written as a product $|\psi\rangle = \otimes_{j=1}^{M} |\psi_j\rangle$, is k-partite entangled when at least one state $|\psi_j\rangle$ contains nonfactorizable k qubits [18,79]. This definition is the same as the entanglement depth [80] [see Fig. 10(c)]. A sufficient condition for $(k + 1)$-partite entanglement stems from the quantum Fisher information F_Q: a state reaching $F_Q[\rho_n, \mathcal{O}] > (sk^2 + r^2)$—where $s = \lfloor n/k \rfloor$ denotes the integer division of n by k, and r is the remainder—is at least $(k + 1)$-partite entangled [18,19].

While F_Q is becoming a useful witness for entanglement in quantum many-body systems [81–86], its origin is as a key figure of merit in quantum metrology, where F_Q quantifies the distinguishability of a state ρ from $\rho' = e^{-i\theta\mathcal{O}} \rho e^{i\theta\mathcal{O}}$, generated by the Hermitian operator $\mathcal{O}$ with infinitesimal θ. Thus, a large F_Q implies a high measurement precision for estimating the value of θ [87,88]. For pure states ψ, the quantum Fisher information becomes simply $F_Q[\psi, \mathcal{O}] = 4\mathrm{Var}(\mathcal{O})_\psi$ [89], whereas for mixed states it provides a lower bound on the variance.

The target state of the QAOA for MaxCut on $\mathcal{G}_n$, the Dicke state, is invariant under a unitary evolution generated by $\hat{L}_z$ but is highly sensitive to rotations around the x or y axes of the collective Bloch sphere [30]. Thus, to obtain a large F_Q, it is advantageous to choose $\mathcal{O} = \hat{L}_x$ or—even more so—$\mathcal{O} = \hat{L}_y$. We report F_Q in Fig. 10(b) for both $\mathcal{O} = \hat{L}_x, \hat{L}_y$ and the resulting k-partite entanglement witnessed by it for the ideal simulations. In this ideal scenario of noiseless numerical

simulations, the large values of $F_Q[\psi, \hat{L}_{x,y}]$ are directly related to the antisqueezing of the final state along the equator of the Bloch sphere.

In the hardware, where the system is no longer in a pure state, it is considerably more challenging to directly access F_Q [81,90]. However, for Gaussian states, one can nevertheless use the empirical relation [30]

$$F_Q/n[\hat{L}_y] \simeq \sigma_{\text{css}}^2/\text{Var}(\hat{L}_z) = 10^{-\mathcal{S}/10} \tag{B1}$$

between F_Q and squeezing. For the simulation, the estimated k using this relation is close to the exact estimation from F_Q in most of cases [see Fig. 10(b)], except for the depth-three QAOA, where the states are no longer Gaussian [27]. Assuming that the above relation holds for depth-one QAOA, where the states are expected to be Gaussian, we obtain the estimates for k-partite entanglement in the hardware implementation reported in Fig. 5(b) of the main text.

APPENDIX C: DISCONTINUITIES IN THE QAOA HARDWARE BENCHMARK

According to Eq. (11), the states in the domain $(\lceil m_- \rceil, \lfloor m_+ \rfloor)$ are included in P_α, where $m_\pm(n, \alpha) = \frac{n}{2} \pm \frac{n}{2}\sqrt{1-\alpha}$. Since $\lfloor m_+ \rfloor$ and $\lceil m_- \rceil$ must both be integers, the span of the domain $\lfloor m_+ \rfloor - \lceil m_- \rceil$ remains constant over a large n range and changes abruptly when $\lfloor \frac{n}{2}\sqrt{1-\alpha} \rfloor \in \mathbb{Z}$ changes value. We denote the values of n at which such changes occur as n_{dis}, which correspond to the discrete jumps along the n axis in Fig. 3(b) of the main text. For $\alpha = 99.9\%$ and n even, we obtain discontinuities in $P_{99.9\%}$ at $n_{\text{dis}} = 64, 128, 190, 254$.

APPENDIX D: OPTIMIZATION METHOD

The 12-qubit example in the main text is run with the QISKIT QAOA Runtime program [39]. To optimize the $\{\gamma, \beta\}$ we use the simultaneous perturbation stochastic approximation (SPSA) algorithm [91] which simultaneously optimizes multiple parameters and can handle noisy environments. We do not initialize the optimizer with values for the learning rate and a perturbation. Instead, we let SPSA calibrate itself in the first 25 iterations. To obtain good solutions we allow SPSA a maximum of 500 iterations and gather a total of 2^{15} shots per iteration.
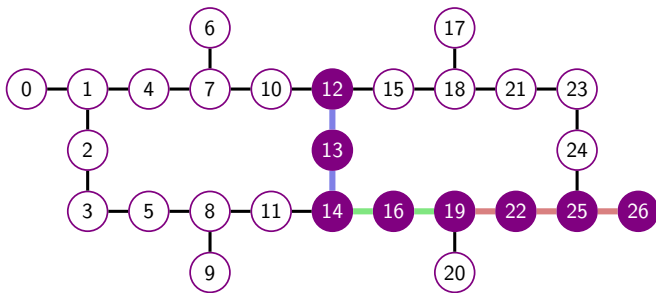

FIG. 11. Coupling map of *ibmq_mumbai* with the qubits used shown in violet. The four-, six-, and eight-qubit data were measured on the linearly connected qubits {19, 22, 25, 26}, {14, 16, 19, 22, 25, 26}, and {12, 13, 14, 16, 19, 22, 25, 26}, respectively, chosen based on the CNOT gate fidelity.

TABLE III. Properties of the relevant CNOT gates as reported by *ibmq_mumbai* on the date of the circuit execution. The average T_1 of the selected qubits is 155 ± 43 μs.

CNOT gate				
Qubit pair	Error (%)	Duration (ns)	Qubit	T_1 (μs)
(12, 13)	0.77	548	12	166
(13, 14)	1.26	320	13	137
(14, 16)	1.04	348	14	174
(16, 19)	0.77	747	16	118
(19, 22)	0.66	363	19	227
(22, 25)	0.58	484	22	122
(25, 26)	0.50	348	25	194
	0.80 ± 0.27	451 ± 155	26	103

APPENDIX E: HARDWARE DETAILS

The superconducting qubit data are gathered on the *ibmq_mumbai* system which has 27 fixed-frequency qubits connected through resonators; its coupling map is shown in Fig. 11. We chose a set of qubits that form a line with the smallest possible CNOT gate error. Each circuit is measured with 4000 shots. The properties of the device such as T_1 times and CNOT gate error are shown in Table III.

APPENDIX F: COMPARISON OF METROLOGICAL GAIN

The squeezing generated by QAOA in the superconducting hardware (see Fig. 5) is comparable to prior trapped-ion works whose aim was to generate highly entangled states (see Fig. 2 of Ref. [10]). Even more, our depth-three QAOA simulations with 12 qubits indicate that, with lower CNOT error rates, superconducting qubit hardware may reach -9.7 dB of squeezing. The same method could also be applied in trapped ions, where the QAOA circuit—thanks to the trapped-ion all-to-all connectivity—is particularly compact (Sec. III C). In addition, our method has a number of advantages over variational *Ansätze* specifically developed for a metrological phase-estimation scenario [25,76–78]. For example, Marciniak *et al.* [25] (i) use a cost function particularly tailored for sensing tasks that optimize the phase sensitivity of their quantum sensor, (ii) use a very general variational *Ansatz* consisting of entangling and decoding unitaries containing rotation once and one-axis twisting operations twice in different directions, following the established knowledge in quantum metrology, and (iii) use a linear phase estimator with an unknown parameter a to estimate the phase from spin measurement, where a also has to be optimized.

By contrast to (i), our cost function is the energy that also creates an entangled state. By contrast to (ii), our variational *Ansatz* is grounded in QAOA, i.e., a Trotterized version of adiabatic computing with a classical optimization that inherits the performance guarantee in the limit $p \to \infty$. By contrast to (iii), our results can be applied to enhance phase sensitivity but are not limited to it. Indeed, the optimization does not include any phase estimator, potentially making the approach useful
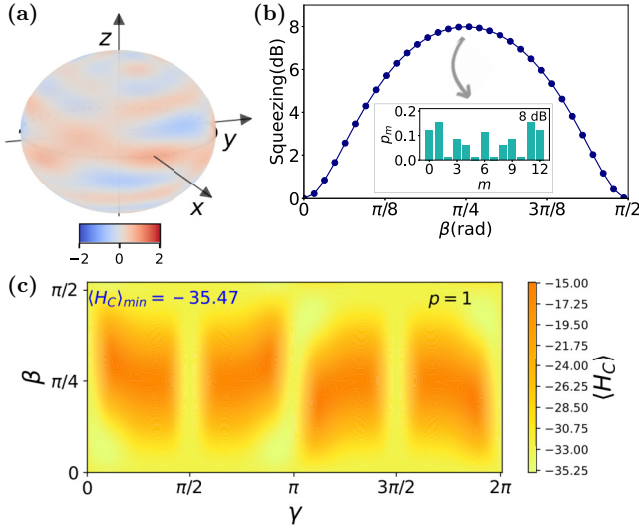
FIG. 12. Illustration of the importance of alternating the cost function and the mixer operator. (a) A fragmented Wigner distribution on the Bloch sphere is obtained when $\hat{H}_C$ is applied with $\gamma = \gamma_1 + \gamma_2 + \gamma_3$ from Fig. 1. (b) For the state in (a) no squeezing is observed at any β. The inset shows the probability distribution at $\beta = \pi/4$, corresponding to $\mathcal{S} = 8$ dB, i.e., over-squeezing. (c) The energy landscape of the depth-one QAOA reveals that the lowest energy it can reach is -35.47, which is inferior to -35.68 obtained in depth-three QAOA.

for other problems while also reducing the number of parameters to optimize. These three points result in a variational form with fewer parameters to optimize than a general variational form and thus is, in principle, easier to optimize. Furthermore, the approach chosen in our paper allows us to benefit from the vast literature on optimizing QAOA parameters, of which the truncated quantum annealing [92] (TQA) initialization is just one example.

APPENDIX G: INCREASING THE DURATION OF $\hat{H}_C$

Squeezing is generated by $\hat{L}_z^2$ [30], which suggests that simply applying $\hat{H}_C \propto \hat{L}_z^2$ for a longer duration, corresponding

to a larger coefficient γ in the QAOA, may transform the coherent state to a squeezed state, after which we can use the mixer $\hat{H}_M$ to reveal the squeezing along $\hat{L}_z$ as in the main text. In this way, one layer of QAOA would suffice to create any squeezing which would also require fewer CNOT gates than when $p > 1$. To test this hypothesis, we run depth-one QAOA using $\gamma = \gamma_1 + \gamma_2 + \gamma_3$ where the γ_i are taken from Fig. 1 in the main text, as they contain the source of "total" squeezing. The result is a fragmented Wigner distribution on the Bloch sphere without observable squeezing in any direction [see Fig. 12(a)]. Furthermore, no squeezing is detected along z for any value of the tomography angle β [see Fig. 12(b)]. This finding is in agreement with the known observation that over-squeezing can be detrimental for precision [93]; however, the states here do not wrap around points near poles because $\hat{L}_z^2$ and $\hat{L}_x$ are not applied simultaneously as in Ref. [93].

APPENDIX H: ADVANTAGES OF MULTILAYER QAOA

One may object to the arguments in Appendix G that the γ we chose is suboptimal. To address that, in Fig. 12(c), we numerically map the energy landscape of depth-one QAOA in the $\{\gamma, \beta\}$ plane. The results reveal a minimum energy of $\langle \hat{H}_C \rangle_{\min} = -35.47$ which corresponds to $|\langle D_6^{12} | \psi \rangle|^2 = 98.53\%$. These results are inferior to those we obtain from the depth-three QAOA, i.e., $\langle \hat{H}_C \rangle_{\min} = -35.68$ and $|\langle D_6^{12} | \psi \rangle|^2 = 99.08\%$. Alternating multiple layers of $\hat{H}_C$ and $\hat{H}_M$ is therefore advantageous over a single application of the one-axis-twisting operator.

To quantify the obtainable improvement as a function of the number of layers used, we can define a new performance metric $\Delta_p^n(\%)$, which compares the energy reduction over the initial *Ansatz* obtained by p layers of QAOA with the one achieved by the ideal target state. In the $n = 12$ case, the initial coherent state and the target Dicke state have $\langle \hat{H}_C \rangle = -33$ and -36, respectively. Thus, a depth-one QAOA (corresponding to the usual squeezing protocol) can reach a maximum $\Delta_1^{12} = 2.47/3$. In contrast, the depth-three QAOA can reach $\Delta_3^{12} = 2.68/3$, as shown in Fig. 1. Thus, according to this metric a depth-three QAOA is $0.21/3 = 7\%$ better than a depth-one QAOA.

APPENDIX I: COMPLEXITY OF OPTIMIZATION LANDSCAPE

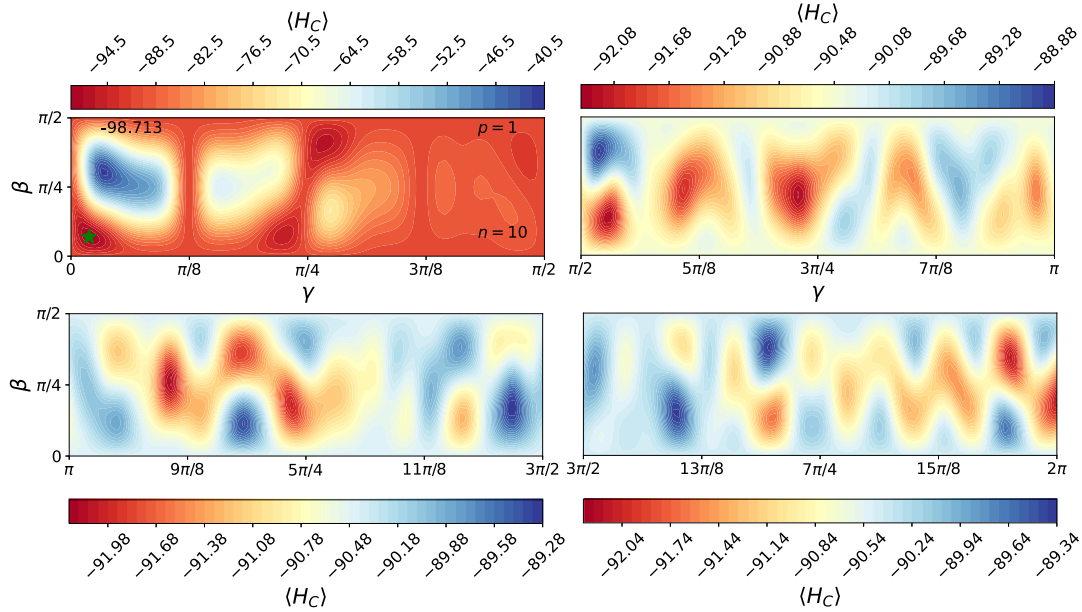Complexity of the optimization landscape is shown in Fig. 13.

FIG. 13. Complexity of the optimization landscape for an $n = 10$ vertices graph with edge weights [3.1, 3.5, 3.9, 3.6, 4.6, 4.2, 4.8, 3.8, 4.1, 4.8, 5.0, 4.8, 4.0, 3.8, 3.2, 4.1, 4.2, 4.6, 4.3, 3.5, 3.9, 3.8, 3.2, 3.2, 4.7, 3.7, 4.1, 3.5, 4.1, 4.0, 4.2, 3.6, 4.4, 4.1, 3.5, 4.2, 3.7, 3.4, 4.4, 4.4, 3.6, 4.0, 4.3, 4.9, 4.1] and QAOA depth $p = 1$. Out of the full landscape, we show the first 0 to 2π portion of the γ landscape in four subplots $\gamma \in [0, \pi/2]$, $[\pi/2, \pi]$, $[\pi, 3\pi/2]$, $[3\pi/2, 2\pi]$ with different color scales to increase the contrast between the local minima and maxima. This reveals a large number of local minima. The small improvement in solution quality with increasing p can therefore be attributed to the many local minima, created from the interference of the frequencies generated by the different edge weights.

[1] E. Farhi, J. Goldstone, and S. Gutmann, A quantum approximate optimization algorithm, arXiv:1411.4028.

[2] P. Torta, G. B. Mbeng, C. Baldassi, R. Zecchina, and G. E. Santoro, Quantum approximate optimization algorithm applied to the binary perceptron, Phys. Rev. B **107**, 094202 (2023).

[3] D. Headley, T. Müller, A. Martin, E. Solano, M. Sanz, and F. K. Wilhelm, Approximating the quantum approximate optimization algorithm with digital-analog interactions, Phys. Rev. A **106**, 042446 (2022).

[4] A. Lucas, Ising formulations of many NP problems, Front. Phys. **2**, 5 (2014).

[5] D. Liang, L. Li, and S. Leichenauer, Investigating quantum approximate optimization algorithms under bang-bang protocols, Phys. Rev. Res. **2**, 033402 (2020).

[6] J. Lee, A. B. Magann, H. A. Rabitz, and C. Arenz, Progress toward favorable landscapes in quantum combinatorial optimization, Phys. Rev. A **104**, 032401 (2021).

[7] M. Streif and M. Leib, Comparison of QAOA with quantum and simulated annealing, arXiv:1901.01903.

[8] J. Wurtz and P. J. Love, Counterdiabaticity and the quantum approximate optimization algorithm, Quantum **6**, 635 (2022).

[9] L. Pezzé and A. Smerzi, Entanglement, nonlinear dynamics, and the Heisenberg limit, Phys. Rev. Lett. **102**, 100401 (2009).

[10] L. Pezzè, A. Smerzi, M. K. Oberthaler, R. Schmied, and P. Treutlein, Quantum metrology with nonclassical states of atomic ensembles, Rev. Mod. Phys. **90**, 035005 (2018).

[11] C. L. Degen, F. Reinhard, and P. Cappellaro, Quantum sensing, Rev. Mod. Phys. **89**, 035002 (2017).

[12] C. Gross, T. Zibold, E. Nicklas, J. Estève, and M. K. Oberthaler, Nonlinear atom interferometer surpasses classical precision limit, Nature (London) **464**, 1165 (2010).

[13] R. J. Sewell, M. Koschorreck, M. Napolitano, B. Dubost, N. Behbood, and M. W. Mitchell, Magnetic sensitivity beyond the projection noise limit by spin squeezing, Phys. Rev. Lett. **109**, 253605 (2012).

[14] L. Barsotti, J. Harms, and R. Schnabel, Squeezed vacuum states of light for gravitational wave detectors, Rep. Prog. Phys. **82**, 016905 (2019).

[15] R. H. Dicke, Coherence in spontaneous radiation processes, Phys. Rev. **93**, 99 (1954).

[16] M. Kitagawa and M. Ueda, Squeezed spin states, Phys. Rev. A **47**, 5138 (1993).

[17] J. Ma, X. Wang, C.-P. Sun, and F. Nori, Quantum spin squeezing, Phys. Rep. **509**, 89 (2011).

[18] P. Hyllus, W. Laskowski, R. Krischek, C. Schwemmer, W. Wieczorek, H. Weinfurter, L. Pezzé, and A. Smerzi, Fisher information and multiparticle entanglement, Phys. Rev. A **85**, 022321 (2012).

[19] G. Tóth, Multipartite entanglement and high-precision metrology, Phys. Rev. A **85**, 022322 (2012).

[20] A. W. Cross, L. S. Bishop, S. Sheldon, P. D. Nation, and J. M. Gambetta, Validating quantum computers using randomized model circuits, Phys. Rev. A **100**, 032328 (2019).

[21] P. Jurcevic, A. Javadi-Abhari, L. S. Bishop, I. Lauer, D. F. Bogorin, M. Brink, L. Capelluto, O. Günlük, T. Itoko, N. Kanazawa *et al.*, Demonstration of quantum volume 64 on

a superconducting quantum computing system, Quantum Sci. Technol. **6**, 025020 (2021).

[22] E. Pelofske, A. Bärtschi, and S. Eidenbenz, Quantum volume in practice: What users can expect from NISQ devices, IEEE Trans. Quantum Eng. **3**, 1 (2022).

[23] V. Giovannetti, S. Lloyd, and L. Maccone, Quantum metrology, Phys. Rev. Lett. **96**, 010401 (2006).

[24] A. Omran, H. Levine, A. Keesling, G. Semeghini, T. T. Wang, S. Ebadi, H. Bernien, A. S. Zibrov, H. Pichler, S. Choi *et al.*, Generation and manipulation of Schrödinger cat states in Rydberg atom arrays, Science **365**, 570 (2019).

[25] C. D. Marciniak, T. Feldker, I. Pogorelov, R. Kaubruegger, D. V. Vasilyev, R. van Bijnen, P. Schindler, P. Zoller, R. Blatt, and T. Monz, Optimal metrology with programmable quantum sensors, Nature (London) **603**, 604 (2022).

[26] J. M. Arrazola, V. Bergholm, K. Brádler, T. R. Bromley, M. J. Collins, I. Dhand, A. Fumagalli, T. Gerrits, A. Goussev, L. G. Helt *et al.*, Quantum circuits with many photons on a programmable nanophotonic chip, Nature (London) **591**, 54 (2021).

[27] D. Gross, Non-negative Wigner functions in prime dimensions, Appl. Phys. B **86**, 367 (2007).

[28] J. Estève, C. Gross, A. Weller, S. Giovanazzi, and M. K. Oberthaler, Squeezing and entanglement in a Bose-Einstein condensate, Nature (London) **455**, 1216 (2008).

[29] T. P. Purdy, P.-L. Yu, R. W. Peterson, N. S. Kampel, and C. A. Regal, Strong optomechanical squeezing of light, Phys. Rev. X **3**, 031012 (2013).

[30] H. Strobel, W. Muessel, D. Linnemann, T. Zibold, D. B. Hume, L. Pezzè, A. Smerzi, and M. K. Oberthaler, Fisher information and entanglement of non-Gaussian spin states, Science **345**, 424 (2014).

[31] W. Muessel, H. Strobel, D. Linnemann, T. Zibold, B. Juliá-Díaz, and M. K. Oberthaler, Twist-and-turn spin squeezing in Bose-Einstein condensates, Phys. Rev. A **92**, 023603 (2015).

[32] K. Xu, Y.-R. Zhang, Z.-H. Sun, H. Li, P. Song, Z. Xiang, K. Huang, H. Li, Y.-H. Shi, C.-T. Chen, X. Song, D. Zheng, F. Nori, H. Wang, and H. Fan, Metrological characterization of non-Gaussian entangled states of superconducting qubits, Phys. Rev. Lett. **128**, 150501 (2022).

[33] A. Sørensen, L.-M. Duan, J. I. Cirac, and P. Zoller, Many-particle entanglement with Bose-Einstein condensates, Nature (London) **409**, 63 (2001).

[34] J. K. Korbicz, I. J. Cirac, and M. Lewenstein, Spin squeezing inequalities and entanglement of *N* qubit states, Phys. Rev. Lett. **95**, 120502 (2005).

[35] J. K. Korbicz, O. Gühne, M. Lewenstein, H. Häffner, C. F. Roos, and R. Blatt, Generalized spin-squeezing inequalities in *N*-qubit systems: Theory and experiment, Phys. Rev. A **74**, 052319 (2006).

[36] O. Gühne and G. Tóth, Entanglement detection, Phys. Rep. **474**, 1 (2009).

[37] G. Tóth, Detection of multipartite entanglement in the vicinity of symmetric Dicke states, J. Opt. Soc. Am. B **24**, 275 (2007).

[38] X. Wang, A. Søndberg Sørensen, and K. Mølmer, Spin squeezing in the Ising model, Phys. Rev. A **64**, 053815 (2001).

[39] J. Weidenfeller, L. C Valor, J. Gacon, C. Tornow, L. Bello, S. Woerner, and D J Egger, Scaling of the quantum approximate

[40] E. Farhi, D. Gamarnik, and S. Gutmann, The quantum approximate optimization algorithm needs to see the whole graph: A typical case, arXiv:2004.09002.

[41] A. Sørensen and K. Mølmer, Quantum computation with ions in thermal motion, Phys. Rev. Lett. **82**, 1971 (1999).

[42] C. A. Sackett, D. Kielpinski, B. E. King, C. Langer, V. Meyer, C. J. Myatt, M. Rowe, Q. A. Turchette, W. M. Itano, D. J. Wineland, and C. Monroe, Experimental entanglement of four particles, Nature (London) **404**, 256 (2000).

[43] B. P. Lanyon, C. Hempel, D. Nigg, M. Müller, R. Gerritsma, F. Zähringer, P. Schindler, J. T. Barreiro, M. Rambach, G. Kirchmair *et al.*, Universal digital quantum simulation with trapped ions, Science **334**, 57 (2011).

[44] M. Werninghaus, D. J. Egger, F. Roy, S. Machnes, F. K. Wilhelm, and S. Filipp, Leakage reduction in fast superconducting qubit gates via optimal control, npj Quantum Inf. **7**, 14 (2021).

[45] A. Wack, H. Paik, A. Javadi-Abhari, P. Jurcevic, I. Faro, J. M. Gambetta, and B. R. Johnson, Quality, speed, and scale: Three key attributes to measure the performance of near-term quantum computers, arXiv:2110.14108.

[46] I. Pogorelov, T. Feldker, Ch. D. Marciniak, L. Postler, G. Jacob, O. Krieglsteiner, V. Podlesnic, M. Meth, V. Negnevitsky, M. Stadler, B. Höfer, C. Wächter, K. Lakhmanskiy, R. Blatt, P. Schindler, and T. Monz, Compact ion-trap quantum computing demonstrator, PRX Quantum **2**, 020343 (2021).

[47] P. Schindler, D. Nigg, T. Monz, J. T. Barreiro, E. Martinez, S. X. Wang, S. Quint, M. F. Brandl, V. Nebendahl, C. F. Roos *et al.*, A quantum information processor with trapped ions, New J. Phys. **15**, 123012 (2013).

[48] E. Magesan, J. M. Gambetta, and J. Emerson, Scalable and robust randomized benchmarking of quantum processes, Phys. Rev. Lett. **106**, 180504 (2011).

[49] E. Magesan, J. M. Gambetta, B. R. Johnson, C. A. Ryan, J. M. Chow, S. T. Merkel, M. P. da Silva, G. A. Keefe, M. B. Rothwell, T. A. Ohki, M. B. Ketchen, and M. Steffen, Efficient measurement of quantum gate error by interleaved randomized benchmarking, Phys. Rev. Lett. **109**, 080505 (2012).

[50] A. D. Córcoles, J. M. Gambetta, J. M. Chow, J. A. Smolin, M. Ware, J. Strand, B. L. T. Plourde, and M. Steffen, Process verification of two-qubit quantum gates by randomized benchmarking, Phys. Rev. A **87**, 030301(R) (2013).

[51] J. L. O'Brien, G. J. Pryde, A. Gilchrist, D. F. V. James, N. K. Langford, T. C. Ralph, and A. G. White, Quantum process tomography of a controlled-NOT gate, Phys. Rev. Lett. **93**, 080502 (2004).

[52] R. C. Bialczak, M. Ansmann, M. Hofheinz, E. Lucero, M. Neeley, A. D. O'Connell, D. Sank, H. Wang, J. Wenner, M. Steffen *et al.*, Quantum process tomography of a universal entangling gate implemented with Josephson phase qubits, Nat. Phys. **6**, 409 (2010).

[53] F. Arute, K. Arya, R. Babbush, D. Bacon, J. C. Bardin, R. Barends, S. Boixo, M. Broughton, B. B. Buckley, D. A. Buell *et al.* (Google AI Quantum and Collaborators), Hartree-Fock on a superconducting qubit quantum computer, Science **369**, 1084 (2020).

[54] M. Benedetti, D. Garcia-Pintos, O. Perdomo, V. Leyton-Ortega, Y. Nam, and A. Perdomo-Ortiz, A generative modeling

approach for benchmarking and training shallow quantum circuits, npj Quantum Inf. **5**, 45 (2019).

[55] P.-L. Dallaire-Demers and N. Killoran, Quantum generative adversarial networks, Phys. Rev. A **98**, 012324 (2018).

[56] A. H. Karamlou, W. A. Simon, A. Katabarwa, T. L. Scholten, B. Peropadre, and Y. Cao, Analyzing the performance of variational quantum factoring on a superconducting quantum processor, npj Quantum Inf. **7**, 156 (2021).

[57] P.-L. Dallaire-Demers, M. Stęchły, J. F. Gonthier, N. T. Bashige, J. Romero, and Y. Cao, An application benchmark for fermionic quantum simulations, arXiv:2003.01862.

[58] P. Schmoll and R. Orús, Kitaev honeycomb tensor networks: Exact unitary circuits and applications, Phys. Rev. B **95**, 045112 (2017).

[59] G. Vidal and C. M. Dawson, Universal quantum circuit for two-qubit transformations with three controlled-NOT gates, Phys. Rev. A **69**, 010301(R) (2004).

[60] D. S. França and R. García-Patrón, Limitations of optimization algorithms on noisy quantum devices, Nat. Phys. **17**, 1221 (2021).

[61] P. Krantz, M. Kjaergaard, F. Yan, T. P. Orlando, S. Gustavsson, and W. D. Oliver, A quantum engineer's guide to superconducting qubits, Appl. Phys. Rev. **6**, 021318 (2019).

[62] M. D. S. Anis, Abby-Mitchell, H. Abraham, A. Offei, R. Agarwal, G. Agliardi, M. Aharoni, I. Y. Akhalwaya, G. Aleksandrowicz, T. Alexander *et al.*, Qiskit: An open-source framework for quantum computing, Version 0.7.2, Zenodo (2019), https://doi.org/10.5281/zenodo.2562111.

[63] Y. Jin, J. Luo, L. Fong, Y. Chen, A. B. Hayes, C. Zhang, F. Hua, and E. Z. Zhang, A structured method for compilation of QAOA circuits in quantum computing, arXiv:2112.06143.

[64] S. Sheldon, E. Magesan, J. M. Chow, and J. M. Gambetta, Procedure for systematically tuning up cross-talk in the cross-resonance gate, Phys. Rev. A **93**, 060302(R) (2016).

[65] N. Sundaresan, I. Lauer, E. Pritchett, E. Magesan, P. Jurcevic, and J. M. Gambetta, Reducing unitary and spectator errors in cross resonance with optimized rotary echoes, PRX Quantum **1**, 020318 (2020).

[66] N. Earnest, C. Tornow, and D. J. Egger, Pulse-efficient circuit transpilation for quantum applications on cross-resonance-based hardware, Phys. Rev. Res. **3**, 043088 (2021).

[67] T. Alexander, N. Kanazawa, D. J. Egger, L. Capelluto, C. J. Wood, A. Javadi-Abhari, and D. C. McKay, Qiskit pulse: Programming quantum computers through the cloud with pulses, Quantum Sci. Technol. **5**, 044006 (2020).

[68] S. Bravyi, S. Sheldon, A. Kandala, D. C. Mckay, and J. M. Gambetta, Mitigating measurement errors in multiqubit experiments, Phys. Rev. A **103**, 042605 (2021).

[69] G. S. Barron and C. J. Wood, Measurement error mitigation for variational quantum algorithms, arXiv:2010.08520.

[70] V. Meyer, M. A. Rowe, D. Kielpinski, C. A. Sackett, W. M. Itano, C. Monroe, and D. J. Wineland, Experimental demonstration of entanglement-enhanced rotation angle estimation using trapped ions, Phys. Rev. Lett. **86**, 5870 (2001).

[71] D. Leibfried, B. DeMarco, V. Meyer, D. Lucas, M. Barrett, J. Britton, W. M. Itano, B Jelenković, C. Langer, T. Rosenband, and D. J. Wineland, Experimental demonstration of a robust, high-fidelity geometric two ion-qubit phase gate, Nature (London) **422**, 412 (2003).

[72] D. Leibfried, M. D Barrett, T. Schaetz, J. Britton, J. Chiaverini, W. M. Itano, J. D. Jost, C. Langer, and D. J. Wineland, Toward Heisenberg-limited spectroscopy with multiparticle entangled states, Science **304**, 1476 (2004).

[73] D. Leibfried, E. Knill, S. Seidelin, J. Britton, R. B. Blakestad, J. Chiaverini, D. B. Hume, W. M. Itano, J. D. Jost, C. Langer *et al.*, Creation of a six-atom 'Schrödinger cat' state, Nature (London) **438**, 639 (2005).

[74] T. Monz, P. Schindler, J. T. Barreiro, M. Chwalla, D. Nigg, W. A. Coish, M. Harlander, W. Hänsel, M. Hennrich, and R. Blatt, 14-qubit entanglement: Creation and coherence, Phys. Rev. Lett. **106**, 130506 (2011).

[75] D. C. McKay, C. J. Wood, S. Sheldon, J. M. Chow, and J. M. Gambetta, Efficient Z gates for quantum computing, Phys. Rev. A **96**, 022330 (2017).

[76] R. Kaubruegger, P. Silvi, C. Kokail, R. van Bijnen, A. M. Rey, J. Ye, A. M. Kaufman, and P. Zoller, Variational spin-squeezing algorithms on programmable quantum sensors, Phys. Rev. Lett. **123**, 260505 (2019).

[77] B. Koczor, S. Endo, T. Jones, Y. Matsuzaki, and S. C. Benjamin, Variational-state quantum metrology, New J. Phys. **22**, 083038 (2020).

[78] J. J. Meyer, J. Borregaard, and J. Eisert, A variational toolbox for quantum multi-parameter estimation, npj Quantum Inf. **7**, 89 (2021).

[79] I. Apellaniz, B. Lücke, J. Peise, C. Klempt, and G. Tóth, Detecting metrologically useful entanglement in the vicinity of Dicke states, New J. Phys. **17**, 083027 (2015).

[80] B. Lücke, J. Peise, G. Vitagliano, J. Arlt, L. Santos, G. Tóth, and C. Klempt, Detecting multiparticle entanglement of Dicke states, Phys. Rev. Lett. **112**, 155304 (2014).

[81] P. Hauke, M. Heyl, L. Tagliacozzo, and P. Zoller, Measuring multipartite entanglement through dynamic susceptibilities, Nat. Phys. **12**, 778 (2016).

[82] J. Smith, A. Lee, P. Richerme, B. Neyenhuis, P. W. Hess, P. Hauke, M. Heyl, D. A. Huse, and C. Monroe, Many-body localization in a quantum simulator with programmable random disorder, Nat. Phys. **12**, 907 (2016).

[83] T.-L. Wang, L.-N. Wu, W. Yang, G.-R. Jin, N. Lambert, and F. Nori, Quantum Fisher information as a signature of the superradiant quantum phase transition, New J. Phys. **16**, 063039 (2014).

[84] S. Yin, J. Song, Y. Zhang, and S. Liu, Quantum Fisher information in quantum critical systems with topological characterization, Phys. Rev. B **100**, 184417 (2019).

[85] G. Mathew, S. L. L. Silva, A. Jain, A. Mohan, D. T. Adroja, V. G. Sakai, C. V. Tomy, A. Banerjee, R. Goreti, Aswathi V. N., R. Singh, and D. Jaiswal-Nagar, Experimental realization of multipartite entanglement via quantum Fisher information in a uniform antiferromagnetic quantum spin chain, Phys. Rev. Res. **2**, 043329 (2020).

[86] P. Laurell, A. Scheie, C. J. Mukherjee, M. M. Koza, M. Enderle, Z. Tylczynski, S. Okamoto, R. Coldea, D. A. Tennant, and G. Alvarez, Quantifying and controlling entanglement in the quantum magnet Cs_2CoCl_4, Phys. Rev. Lett. **127**, 037201 (2021).

[87] S. L. Braunstein and C. M. Caves, Statistical distance and the geometry of quantum states, Phys. Rev. Lett. **72**, 3439 (1994).

[88] G. M. Tino and M. A. Kasevich, Quantum theory of phase estimation, in *Atom Interferometry: Proceedings of the International School of Physics "Enrico Fermi", Course 188,*

Varenna on Lake Como, Villa Monastero, 15–20 July 2013, International School of Physics Enrico Fermi Series (IOS Press, 2014).

[89] G. Tóth and I. Apellaniz, Quantum metrology from a quantum information science perspective, J. Phys. A: Math. Theor. **47**, 424006 (2014).

[90] R. Costa de Almeida and P. Hauke, From entanglement certification with quench dynamics to multipartite entanglement of interacting fermions, Phys. Rev. Res. **3**, L032051 (2021).

[91] J. C. Spall, An overview of the simultaneous perturbation method for efficient optimization, Johns Hopkins APL Tech. Dig. **19**, 482 (1998).

[92] S. H. Sack and M. Serbyn, Quantum annealing initialization of the quantum approximate optimization algorithm, Quantum **5**, 491 (2021).

[93] H. Strobel, Fisher information and entanglement of non-Gaussian spin states, Ph.D. thesis, Kirchhoff Institute for Physics, Universität Heidelberg, 2016, https://archiv.ub.uni-heidelberg.de/volltextserver/20251/.